Environ. Sci. Technol. **1998**, *32,* 2531−2541

Structural Changes in a Dissolved Soil Humic Acid during Photochemical Degradation Processes under O_2 and N_2 Atmosphere

PHILIPPE SCHMITT-KOPPLIN,*,† NORBERT HERTKORN,† HANS-ROLF SCHULTEN,‡ AND ANTONIUS KETTRUP†

GSF—National Research Center for Environment and Health, Institute for Ecological Chemistry, Ingolstädter Landstrasse 1, D-85764 Neuherberg, Germany, and Institut Fresenius, Chemical and Biological Laboratories, Im Maisel 14, D-65232 Taunusstein, Germany

Irradiation (UV/Vis $\lambda > 290$ nm) under nitrogen and oxygen atmosphere significantly affected the structure of dissolved humic material (DHM). Photobleaching of the DHM solution occurred essentially under O_2 atmosphere in conjunction with a decrease in average molecular weight and an increase in acidity due to the disaggregation and photooxidation processes. The structural changes were followed by various separation and analytical methods including capillary zone electrophoresis (CZE), gel permeation chromatography (GPC), Fourier transformation infrared (FTIR), and one- and two-dimensional nuclear magnetic resonance spectroscopy (NMR) as well as pyrolysis-field ionization mass spectrometry (Py-FIMS). The structural investigations showed selective degradations of DHM, especially under oxygen atmosphere. Structures of lignic and lipidic origin were the most photolabile as compared to carbohydrates, alkylbenzenes, or N-containing structures that accumulated in the system. Under nitrogen atmosphere the acids remained fairly stable. Indirect photolysis seems to be the major pathway in degradation of DHM subjected to UV/Vis irradiation.

Introduction

Dissolved humic materials (DHM) are the main constituents of the dissolved organic carbon (DOC) pool in surface waters (freshwaters and marine waters), groundwaters, and soil porewaters and commonly impart a yellowish-brown color to the water system. Despite the different origins responsible for their main structural characteristics, they all constitute refractory products of chemical and biological degradation and condensation reactions of plant or animal residues and play a crucial role in many biogeochemical processes. They all are known to be among the most important natural sunlight absorbing components of soil surfaces and aquatic environments and constitute about half of the organic and nearly all of the colored matter in all of the different natural environments (*1*−*3*). Soil humic substances generally differ from freshwater humic substances in their elemental and functional group composition; they are typically of higher molecular weight, of lower carboxylic and higher phenolic content and the ratio of extractable humic to fulvic acid is frequently higher (*1*). Freshwater humic substances contain stronger acidic functions due to the presence of keto acid and aromatic carboxyl-group structures (*4*−*6*), and marine humic substances lack lignin constituents and are of rather aliphatic and peptide origin coming from non-lignin-containing organisms (*7*). Despite these structural differences, all humic substances contain a variety of active chromophores at wavelengths found in the surface solar spectrum; most prominent are aromatic systems as well as conjugated carbonyl derivatives.

The anticipated increase in the global UV radiation resulting from a reduced ozone content in the stratosphere requires a better understanding of the UV-mediated chemical processes taking place with DOC in ecosystems (*8*−*11*). Photochemical degradation of refractory organic matter constitutes an important proportion of the global carbon cycling (*11, 12*). Photomineralization generating small molecules such as H_2O, CO, and CO_2 (*13*) and photochemical breakdown into biologically utilizable carbonyl compounds (*11, 14*−*46*) both contribute to the loss of refractory organic carbon from the ecosphere.

Photochemically mediated processes are important in most, if not all, areas of aqueous-phase environmental chemistry, and natural DHM present in ecosystems undergoes a complex array of primary and secondary photoprocesses when exposed to sunlight. Numerous studies have been performed to assess the environmental relevance of photochemical degradation pathways for xenobiotica and natural organic matter (*17, 18*). Humic materials are known to affect the photodegradation of pollutants, either acting as a photosensitizer or as absorbing (and light attenuating) chromophor (*19*−*22*) depending on their chemical structure (*23*−*26*).

Studies of the light-induced changes in the spectral properties of natural organic matter have shown that humic substances are faded by exposure to UV and visible light (*27*−*31*). The acceleration of fading in the presence of dioxygen (*32*) and the retardation in the presence of N_2 (*33*) have also been reported. Little information is available about the nature of the oxidizing species that are involved in the fading and the possible role of these light-induced reactions in the cycling of carbon or nitrogen in the environment [production of CO_2 and CO (*13*), NO_2, NO_3^-, and NH_4^+ (*34*)]. Several studies report on changes affecting the molecular weight repartition of humic material during photodegradation (*35, 36*) or the production of low molecular weight organic acids (*15, 37, 38*) responsible for the enhancement of the biological activity of the waters. These studies, like most of the research on photoreactions involving natural organic matter so far, provide only limited understanding of the selective degradation of the chromophores or the products generated by photolysis.

In the present study, we investigated in detail the composition and structural changes of a soil humic acid occurring during UV/Vis irradiation under nitrogen and oxygen atmosphere in laboratory irradiation conditions in aqueous solution. The soil humic substance was selected because it was a very well-defined reference material, which our group has utilized in several studies (*23, 39*−*41*).

* Corresponding author tel: 08161 987720; fax: 08161 81612; e-mail: SCHMITTPH@GSF.de.
† Institute for Ecological Chemistry.
‡ Institut Fresenius.

S0013-936X(97)00636-6 CCC: $15.00
Published on Web 07/22/1998

Materials and Methods

Extraction Procedure. Humic materials employed in this study were isolated from an air-dried and sieved (2 mm) standard soil (A_p horizon: 0−20 cm; 1.36% organic C; pH 6.0; 9.71 C/N) of a cultivated loamy brown soil from the FAM location (Forschungsverbund Agrarökosystem München) in Scheyern-South Germany (sampling points 290/190 and 270/190) (*40*). The extraction and purification procedures followed the guidelines of the International Humic Substances Society (IHSS). Briefly, 100 g of soil was shaken for 1 h at room temperature with 1 L of 1 M HCl to remove alkali earth and free carbonates. After centrifugation (supernatant: fulvic acid FA1), the residue was neutralized with 1 M NaOH to pH 7, and 1000 mL of 0.1 M NaOH was added to give a suspension that was shaken for 4 h under nitrogen atmosphere. The alkaline supernatant obtained by centrifugation was acidified with 6 M HCl and kept at room temperature overnight. Coagulate (humic acid HA) and the supernatant (fulvic acid FA2) were separated by centrifugation. To remove suspended clays, the HA was dissolved in a minimum volume of 0.1 M KOH under N_2 and the ionic strength adjusted to 0.3 M K^+ by adding KCl, followed by 1 h of centrifugation. After acidification with 6 N HCl and centrifugation, the coagulate HA was shaken with 100 mL of a HCl/HF solution (0.1 M HCl and 0.3 M HF) to reduce the ash content. Humic acids were then protonated by cation exchange on Dowex 50WW×8. Following preconcentration on XAD8 resin, the FA1 and FA2 fractions were combined to give the fulvic acid, which was like HA subjected to HF/HCl treatment, followed by protonation. The H^+-saturated humic substances were then freeze-dried.

Irradiation Experiments. A total of 50 mg of H^+-saturated humic acids was dissolved in 250 mL of distilled water to reach a concentration of 200 mg/L by ajusting the pH to 6.8 with 0.1 N NaOH. This solution was placed in a cylindrical vessel and a Philips HPK 125 W high-pressure mercury vapor lamp [light intensity; 4.75×10^3 lm (*42*)], with a cooled Pyrex housing to block wavelengths shorter than 290 nm was inserted. N_2 and O_2 were bubbled through a sintered glass frit from the bottom of the vessel maintaining saturation throughout the irradiation time for a total of 30 h (*23*). The reaction temperature under these conditions was 22 ± 2 °C. Aliquots of 2 mL were repeatedly sampled during irradiation and kept in the refrigerator. After finishing irradiation, the remaining humic acids solutions were freeze-dried and kept in glass vials for future analysis.

Analytical Methods Used during Irradiation. Total organic carbon (TOC) was measured from aliquots and diluted with deionized water (1/4; v/v) using a Shimadzu TOC-5000. The pH of each aliquot was measured using a Radiometer Copenhagen PHM82 standard pH-meter. UV/Vis spectra were recorded with a SP8-100 UV/Vis spectrometer PYE (UNICAM). Gel permeation chromatography (GPC) was performed using a Latec LC column with TSK 55s gel (27 cm × 2.5 cm i.d.) employing a phosphate buffer at pH 7 (3.52 g/L KH_2PO_4 + 7.56 g/L Na_2HPO_4) at a flow of 2 mL/min. Standard proteins were used for the calibration curve [cytochrome *c*, myoglobin, carbonic anhydrase, ovalbumin, ovotransferrin, lactate dehydrogenase (Merck)], and this GPC procedure was sufficient to follow the relative changes in average molecular weight of the humic acid during photolytic process.

Analytical Methods Used after Irradiation. Weight loss was measured after freeze-drying of irradiated solutions. Elemental analysis was performed with a CHN-1106 analyzer from Carlo Erba Instruments. E_4/E_6 ratios were measured from solutions of freeze-dried substances in 0.1 M NaOH (1 mg/L). After a 30-min equilibration time in 20 mL of 1 N KCl (equilibration pH), 5 mg of freeze-dried substances was subjected to potentiometric titrations with 0.01 M NaOH under N_2 atmosphere. Capillary zone electrophoresis was performed with a Beckman PA/CE system 2050 employing a 50 mM acetate buffer at pH 5.3 in a silica fused capillary (i.d. 75 μm, total length: 57 cm, 50 cm to detector) under a voltage of 20 kV at 30 °C (*43*).

Infrared spectra (FTIR) were recorded from KBr pellets with a Perkin-Elmer System 2000. KBr pellets were produced by mixing 1 mg of freeze-dried substances with 200 mg of KBr. Resolution enhancement using the standard software (deconvolution factor 50, smooth factor 30) was utilized to define wavenumbers of prominent bands. The 10-mL irradiated and nonirradiated solutions were extracted twice with 10 mL of *n*-hexane and after preconcentration to 1 mL were subjected to GC/MS analysis (HP5MS column, 30 m × 0.25 mm × 0.25 μm); 120 °C isotherm 5 min, 4 °C/min up to 250 °C, isotherm 250 °C for 30 min; Hewlett-Packard 5890 Series II Plus gas chromatograph coupled to a FID detector and a 5989 A MS-Engine).

Solution (0.1 N NaOD in D_2O, 303 K) NMR spectroscopy was performed on a Bruker AC 400 NMR spectrometer operating at 400.13 MHz (^{1}H) and 100.77 MHz (^{13}C) utilizing a broadband 5-mm probe for ^{13}C NMR and an inverse geometry 5-mm broadband probe for ^{1}H NMR spectra, respectively. Qualitative carbon NMR spectra have been recorded in 0.1 N NaOD using a pulse sequence with reduced acoustic ringing (*44*) under the following conditions: D1, 1.5 s; AQ, 0.4 s; 90°, 7.5 μs; exponential line broadening, 75 Hz and proton NMR spectra with the first increment of the NOESY-presat sequence [D1, 2s; AQ, 1.2 s; 90°, 8.3 μs; LB, 1s (*45*)] for water suppression centered at the residual HDO resonance [reference for all NMR spectra: $\delta_{HDO/NaOD} = 4.63$ ppm; ^{13}C reference: CH_3OH in D_2O (external): $\delta = 49.00$ ppm]. Semiquantitative ^{13}C NMR spectra (*46*) were recorded at 125 MHz on a Bruker DMX 500 spectrometer with a 5-mm broadband probe under the following conditions: D1, 3.5 s; AQ, 0.4 s; 45°, 5.4 μs; exponential line broadening, 75 Hz. Two-dimensional NMR spectra of humic substances were acquired on a Bruker DMX 500 spectrometer (^{1}H frequency, 500.13 MHz) with an inverse 5-mm probe equipped with actively shielded gradient coils (gradient system BGU II, amplifier BPU 10). Gradient-enhanced (gradient pulse, 1 ms; gradient recovery, 500 μs) phase-sensitive (TPPI) HMQC spectra were registered with GARP-^{13}C decoupling (90°, 70 μs). A total of 512 scans each (d1, 1.5 s) with a resolution of 2K data points in F2 [F2(^{1}H): AQ, 0.2 s; SW, 5000 Hz; 90°, 10.8 μs; exponential multiplication, 35 Hz] and 256 increments [F1(^{13}C): SW, 20000 Hz; 90°, 10 μs; shifted sine bell, $\pi/4$; zero filled to 512 increments corresponding to a digital resolution in F1, 39.1 Hz] were acquired, assuming an average direct ^{13}C,^{1}H-coupling constant of 150 Hz (d2, 3.33 ms). Magnitude HH−COSY and GS−HH−COSY spectra were acquired with 32 scans each (d1, 1.5 s) with a resolution of 1K data points in F2 [F2(^{1}H): AQ, 93 ms; SW, 5482 Hz; 90°, 10.8 μs; unshifted sine bell in F2 and F1] and 256 increments, corresponding to a digital resolution in F1, 21.4 Hz (gradient pulses and delays used as above).

For temperature-resolved Py-FIMS, about 200 μg of humic substances were thermally degraded in the ion source of a MAT731 (Finnigan, 28127 Bremen, Germany) mass spectrometer. The samples were weighted before and after Py-FIMS (error ± 10 μg) to determine the pyrolysis residue and the produced volatile matter. All samples were heated in high vacuum (1.3×10^{-4} Pa) from 323 to 973 K at a heat rate of approximately 0.5 K s^{-1}. About 60 magnetic scans were recorded for the mass range m/z 16−1000. In general, at least three replicates were performed for each sample. The total ion intensities (TII) of the single spectra were normalized to 1 mg sample weight, averaged for replicate runs, and plotted versus the pyrolysis temperature, resulting

TABLE 1. Elemental Analyses of HA, FA, and Irradiated Substances HAN_2 and HAO_2

	C %	H %	N %	O %	ash %	C/N	N/C	O/C	H/C
HA	48.30	4.04	4.44	39.52	3.70	10.88	0.09	0.61	1.00
FA	44.71	3.44	2.59	43.26	6.00	17.26	0.06	0.73	0.92
HAO_2	34.73	3.38	4.13	44.86	12.90	8.41	0.12	0.97	1.17
HAN_2	42.59	3.59	3.72	40.90	9.20	11.45	0.09	0.72	1.01

in Py-FIMS thermograms. For the selection of biomarkers and quantitative evaluations, detailed descriptions of the method have been published (*47*).

Results and Discussion

Changes followed during the Photodegradation. The dissolved humic substances (DHS) were irradiated under nitrogen and oxygen atmosphere for 30 h, and the content of dissolved organic carbon was followed by TOC measurements. Under nitrogen, the TOC remained nearly constant, but under oxygen the TOC decreased monotonically by 43% of its initial value within 30 h. However, the corresponding weight loss was 8% (N_2) and 20% (O_2), respectively. Monitoring of the pH during irradiation revealed no change under nitrogen in contrast to oxygen atmosphere, where the pH decreased by 2 units to 4.8.

The weight loss during irradiation can be attributed to loss of volatiles formed and extrusion of small molecules such as CO_2, CO, and H_2O. Under oxygen atmosphere the weight loss is significantly attenuated as compared to the reduction in TOC content; the small added amount of 0.1 N NaOH to reach initial pH of 6.8 does not explain this relative high weight. This implies significant changes in the chemical structure with the added weigth plausibly introduced by oxidation. Oxidation of the humic substance is also indicated by an increase of the O/C ratio from 0.61 to 0.97 (Table 1). The pH reduction upon irradiation under oxygen indicates the formation of carboxylic groups as confirmed by FTIR, NMR, and Py-FIMS analysis.

Oxidative chemical degradation of humic substances predominantly gives fatty acids, aliphatic and aromatic carboxylic, and phenolic and benzenecarboxylic acids (*32, 36, 48*). Our comparative GC−MS measurements of the hexane extracts of the DHS fractions confirmed the production of benzenedicarboxylic acids as well as long chain alkanes (C_{2n}, $n = 7-12$) preferentially in humic acids irradiated under oxygen.

The relative increase in ash content for HAN_2, which is even more pronounced under oxygen atmosphere, is due to the addition of 0.1 N NaOH added to the initial solution to reach the pH of 6.8; referring to the observed weight loss, this indicates a photomineralization of organic material under O_2 and subsequent accumulation of the inorganic salts. A minor growth of the O/C ratio under nitrogen corresponds to a relative increase of less photoreactive oxygen containing functional groups. The increase in the H/C ratio under oxygen is caused by photodegradation of aromatic constituents (as confirmed by ^1H NMR) while it remains almost constant under nitrogen. The decreasing C/N ratio indicates a relative photostability of the nitrogen-containing functional groups, which is corroborated by the results of Py-FIMS. Under nitrogen atmosphere, the C/N ratio slightly increases; this may be correlated with radical stabilizing properties of the electronegative nitrogen in aromatic (and nitroxide) structures. The primary radicals then decompose more quickly than other partial structures.

The molecular size distribution was also found to decrease during irradiation, indicating a degradation to smaller fragments (Table 2). Under nitrogen, a continuous decrease in average molecular weight (AMW) is found.

TABLE 2. TOC, pH, Molecular Weight (MW), and Absorbance at 465 nm Evolution during Photodegradation of Humic Substances under O_2 and N_2 Atmosphere

time (h)	TOC (mg/L)	pH	AMW (kD)[a]	abs. 465 nm
O_2				
0	48.8	6.80	19.2	0.134
5.3	43.7	5.65	8.8	0.084
10	42.8	5.30	7.0	0.063
19.5	38.8	4.88	6.4	0.036
25.8	35.2	4.85	5.5	0.038
30	27.8	4.84	4.2	0.038
N_2				
0	49.5	6.82	17.9	0.132
4	48.8	6.80	16.2	0.134
9	49.0	6.80	17.8	0.133
12	48.0	6.80	15.9	0.133
17.25	47.0	6.80	16.0	0.134
31	48.9	6.80	13.3	0.120
weight before irradiation			40.0 mg (100.0%)	
weight after irradiation O_2			32.1 mg (80.3%)	
weight after irradiation under N_2			36.8 mg (92.0%)	

[a] Repetitive measurements show AMW variations of less than 10%.

TABLE 3. Average Molecular Weight (AMW), E_4/E_6 Ratio, pH_{equ} (in mequiv of NaOH Added) and Average Electrophoretic Mobility (AEM) of HA, FA, and Irradiated Substances

	E_4/E_6	AMW (kD)	total acidity	AEM ($cm^2/V\ s$)[a]
HA	5.52	17.4	2.58	-2.67×10^{-4}
FA	18.00	9.4	4.00	-3.11×10^{-4}
HAO_2	13.20	4.2		-2.80×10^{-4}
HAN_2	4.57	13.3		-2.73×10^{-4}

[a] EOF at 4.75×10^{-4} cm^2/V s.

Under oxygen the decrease in AMW is much more pronounced and apparently follows a two-step process: a sharp decline to half of the initial MW within the first 5 h is followed by a monotonuous diminution that resembles the course of the AMW under nitrogen. This indicates a two-step procedure of structural changes within the humic aggregate structure: a fast disaggregation is followed by photodegradation of the constituents. The fast disaggregation may be initiated by oxidative cleavage of hydrogen bonding functions and easily oxidizable phenolic linkages.

The E_4/E_6 ratios [ratio of the absorbance at 465 nm to absorbances at 665 nm (*49*)] of freeze-dried substances were found to inversely correlate with AMW (Table 3). Under oxygen conditions, the highly condensed HA with low E_4/E_6 ratio evolves to a fulvic-like system with a high E_4/E_6 ratio. The E_4/E_6 ratio of HAN_2 decreases slightly, reflecting the combined effect of slow AMW decrease and rapid decarboxylation.

The progression of the AMW corroborates a more extensive degradation under oxygen than nitrogen. Further structural changes are revealed by the correlation of the absorption at 465 nm with the TOC content. Under oxygen, TOC and AMW are continuously decreasing whereas the absorbance at 465 nm reaches a steady state after 20 h of irradiation, which has then declined to 28% of its initial value. In conjunction with the TOC and AMW variations, this indicates continuous photooxidation and mineralization while maintaining a steady state of the absorbance.

Capillary Zone Electrophoresis (CZE). After lyophilization, the samples were dissolved in 0.1 N NaOH and subjected to capillary zone electrophoresis (CZE). CZE has successfully found applications in biochemistry and achieves separation of charged molecules based on their relative electrophoretic

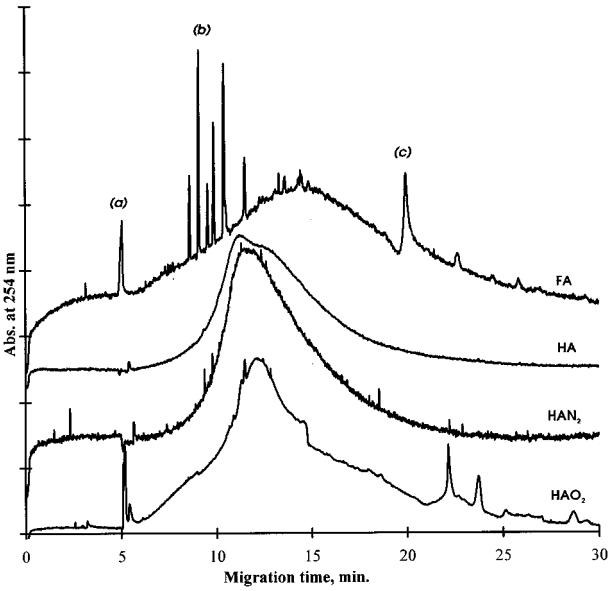

FIGURE 1. CZE electropherograms of FA, HA, HAN_2, and HAO_2: (a) neutral components; (b) phenolic acid region; (c) high charge density region.

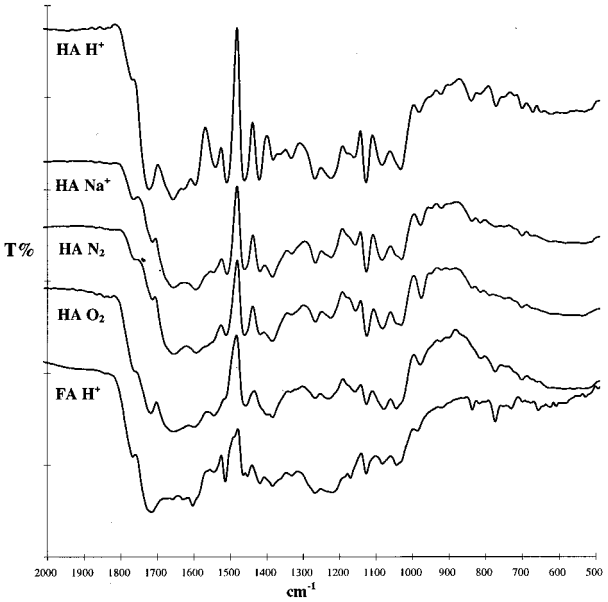

FIGURE 2. FTIR spectra of HAH^+, $HANa^+$, HAN_2, HAO_2, and FAH^+.

mobility under a chosen electric field. The electrophoretic migration of humic substances subjected to this analytical technique is not solely governed by their charge but also by their conformation (size) at the applied pH (*43*). An acetate buffer at pH 5.3 was chosen to ensure a good separation in CZE fingerprints of humic and fulvic acids. Under these conditions, the electropherograms of the humic acids show a Gaussian repartition of the charge densities around an average electrophoretic mobility (AEM) of negatively charged molecules. Neutral molecules [(a) in Figure 1] are indicators for the electroosmotic flow (EOF) governing the speed of uncharged molecules in the capillary as function of experimental conditions (pH, *T*, buffer composition). The measured average electrophoretic mobilities AEM_{mes} ($cm^2/V\ s$) are calculated taking account of the electrophoretic velocity v_e (cm/s) and the applied electric field strength E (V/cm): $AEM_{mes} = v_e/E = (L_d/t_m)/(V/L_t)$ [with L_d, length of the capillary to the detector, 50 cm; L_t, total length of the capillary, 57 cm; V, the applied voltage, 20000 V; t_m, migration time, s]. The absolute AEM is calculated relative to the EOF: AEM = EOF − AEM_{mes}.

From Figure 1, it is deduced that no significant changes in the electrophoretic behavior affected HAN_2 as compared to HA. The AEM of the humic substances are given in Table 3. The HAO_2 fraction gives a different fingerprint and AEM as compared to the initial HA fraction, more resembling the fulvic acids, with unassigned but individual sharp peaks originating from molecules with high charge-to-mass ratios [(c) in Figure 1]. The enhanced contribution of neutral molecules present only in the electropherograms of HAO_2 and FA is noticed. Fulvic acids show a higher AEM than humic acids due to their higher polydispersity and charge-to-mass ratio (smaller AMW and stronger acidities/more acidic functionalities). The isolated sharp peaks at low migration times typical of FA fingerprints [(b) in Figure 1] are neither found in HA nor in HAN_2 and correspond to low molecular weight phenolic acids (vanillic acid, *p*-hydroxybenzoic acid) as confirmed by coelectrophoresis and by comparison of the respective UV spectra. The CZE electropherograms show that under oxygen conditions the irradiation of the monodisperse humic acid system leads to the formation of ionizable subunits of polydisperse character comparable to fulvic acids, confirming the already exposed E_4/E_6, potentiometric titration, and gel permeation data.

Fourier Transform Infrared Spectroscopy (FTIR). Infrared spectroscopy has long been used for the structural studies of humic substances, particularly for defining the nature of oxygen in organic molecules. Qualitative variations within different regions of the IR spectrum of the photoproducts are observed (*50*). The intensity changes observed are better revealed by resolution enhancement methods (deconvolution) and difference spectroscopy (*33*).

Figure 2 shows the FTIR spectra of H^+ and corresponding Na^+ humic acids (HAH^+ and $HANa^+$). The $HANa^+$ is the reference and was obtained by freeze-drying the pH 6.8 adjusted 200 mg/L HA nonirradiated solution. The alterations in the intensities of the 2400−2700, 1726, 1421, 1221, and 1182 cm^{-1} bands (COOH) are directly related to the increase of the carboxylate 1560 and 1400 cm^{-1} bands (COO^-). No significant difference could be observed between the HAN_2 and the Na^+HA. Compared to HAN_2, the irradiation under O_2 atmospheric conditions causes bands 1773, 1722, 1545 and 1402 cm^{-1} to increase and bands at 3070, 1600, 1508, 1464, 1420, 1333, 1268, 1132, 1029, and 981 cm^{-1} to decrease.

In addition, the intensity of the 1520−1545 cm^{-1} band is increasing during photooxidation (amide II region) while the 3070 and 1508 cm^{-1} bands are decreasing (CH aromatic region), confirming Py-FIMS and NMR data.

^1H and ^{13}C Nuclear Magnetic Resonance Spectroscopy (NMR). NMR spectroscopy is typically utilized for the structural analysis of humic substances by integrating one-dimensional ^1H and ^{13}C NMR spectra. Distinct ranges of chemical shift are then attributed to a specified set of chemical environments such as aliphatic, heteroatom-substituted, or aromatic positions.

We have divided the chemical shift range of the proton NMR spectra into five groups of chemical environments (δ-scale, Table 4): (0−1.2) terminal methyl groups and unfunctionalized aliphatics, (1.2−1.9) aliphatic protons β and γ to keto or aromatic groups, (1.9−3.1) aliphatic protons α to keto or aromatic groups, (3.1−5.0) aliphatic protons α to heteroatoms (oxygen and nitrogen), and (6.3−8.4) aromatic protons (*51*). Similarly the carbon NMR spectra have been divided into the seven groups specified in Table 4.

The main difference in the proton NMR spectra of original and irradiated samples is a relative decrease in aliphatic and an increase in carbohydrate constituents. In HAO_2, a substantial (50%) decrease of aromatic protons is found with

TABLE 4. Chemical Shifts Ranges in ^{13}C and ^{1}H NMR and Their Relative Contribution (%) for HA, HAO_2, HAN_2[a]

δ (^{1}H) (ppm)	HA	HAO_2	HAN_2	
0−1.2	13.0	11.6	11.3	methyl
1.2−1.9	25.7	23.0	22.9	aliphatic
1.9−3.1	20.1	26.0	21.8	functionalized aliphatic
3.1−4.7	30.5	34.9	33.8	heteroatom substituted
6.3−8.4	10.7	4.9	10.3	aromatic
δ (^{13}C) (ppm)	HA	HAO_2	HAN_2	
0−50	23.3	20.9	21.5	aliphatic
50−65	8.8	10.2	11.0	methoxy, N-alkyl
65−105	17.7	15.7	15.0	heteroatom substituted
105−145	28.1	22.0	29.1	C,H aromatic
145−165	5.9	4.8	6.2	O,N aromatic
165−185[b]	15.1	24.0	16.0	carboxy, amides, esters
185−220	1.1	2.4	1.1	keto

[a] Integrals taken from 400 MHz ^{1}H NMR and 125 MHz ^{13}C NMR spectra. [b] A tiny fraction of C1 phenoxides may resonate between 165 and 168 ppm.

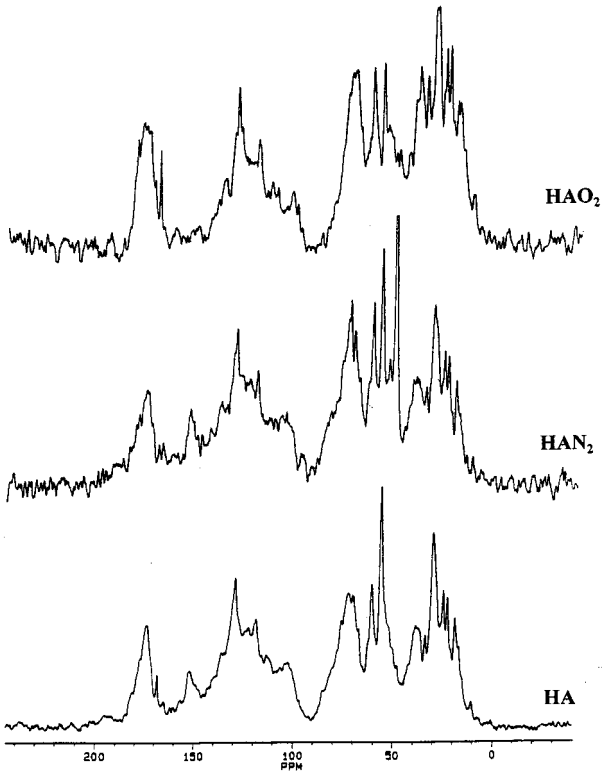

FIGURE 3. ^{13}C NMR spectra (100 MHz) of HA, HAN_2, and HAO_2.

all protons within the aromatic range of chemical shifts equally affected; therefore, from the ^{1}H NMR data alone a significant selectivity of the photodegradation within the aromatic systems cannot be deduced (Table 4). Only in the 500 MHz ^{1}H NMR spectrum some marginal alterations within the aromatic section are visible (see Figure 6).

Major changes in the carbon NMR spectra are visible in the regions of the chemical shift downfield from 140 ppm (Figure 4) and at 20−30 ppm, respectively. In HAO_2, the amount of carboxy groups resonating at 170 ppm is substantially (approximately 150%) more intense than in HAN_2, but the distinct resonance in the range 140−155 ppm, present in HA and preserved in HAN_2, has almost completely disappeared (Figures 3 and 4). The low field region of the 125 MHz ^{13}C NMR spectrum of HAO_2 indicates resynthesis of carboxylic derivatives and ketones as well (Figure 4). In the aliphatic region of the chemical shifts, resonances in the

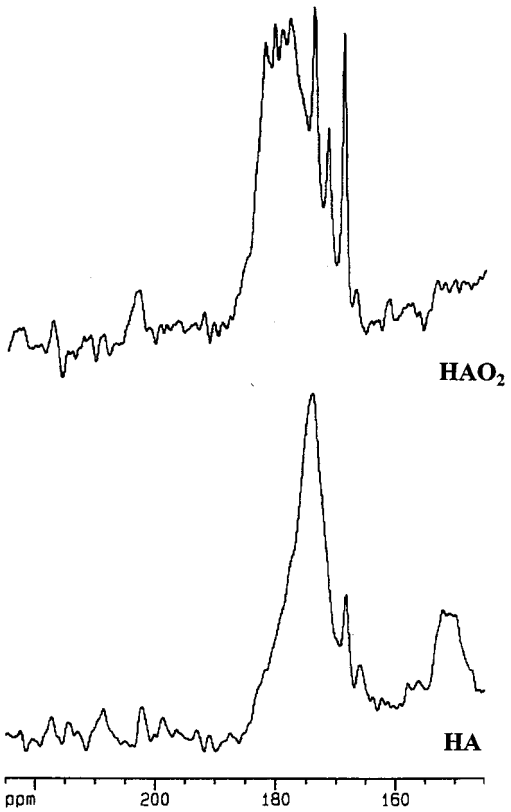

FIGURE 4. ^{13}C NMR spectra (125 MHz) of HA and HAO_2, low field section.

range 20−30 ppm are substantially decreased in HAN_2. These results confirm an extensive photodegradation of phenolic subunits as well as a substantial synthesis of carboxy acids under oxygen atmosphere.

Two-Dimensional Nuclear Magnetic Resonance Spectroscopy (2D NMR). Two-dimensional NMR spectroscopy is a general concept providing more detailed information by introducing a second independent frequency variable. The second frequency domain available in 2D NMR spectroscopy provides information concerning spatial or bonding interactions between pairs of atoms (*45*). The main objective of 2D NMR is the elucidation of connectivity patterns. 2D NMR in the form of heteronuclear shift correlation spectroscopy offers a variety of ways to identify directly bonded and long-range pairs of different atoms. Far-reaching structural constraints are deduced, and information from one spectrum is helpful in the assignment of the other spectrum (*45, 52*).

$^{13}C,^{1}H$-heteronuclear chemical shift correlated spectroscopy allows a more precise characterization of humic substances, and it is preferentially acquired with enhanced sensitivity (*45, 52*) by proton detection [HMQC, heteronuclear multiple-quantum coherence spectroscopy (*45*)] rather than by the traditional carbon detection (HETCOR, heteronuclear correlated spectroscopy). An efficient way of water suppression in proton-detected 2D NMR spectra of humic substances is provided by means of gradient-echo spectroscopy (*45*), which gives superior results in the elimination of residual water resonances when compared with presaturation. This technique has not yet been applied for the structural analysis of humic substances (*53, 54*).

Cross-peaks in H,C HMQC spectra represent single bonds between carbon and proton atoms. Compared to 1D NMR, ^{1}H and ^{13}C NMR spectra, HMQC spectra provide highly resolved information about protonated carbon atoms in humic substances.

TABLE 5. Prominent Cross Signals in the HMQC Spectra of Humic Materials

cross-peak	$\delta(^{13}C)$	$\delta(^{1}H)^{a}$	tentative assignment
M_1	10.6	0.8	H_3C-b carbonyl substituted
M_2	14.5	0.8	H_3C-terminal in a long aliphatic chain
M_3	18.5	0.8	H_3C-C(=O)—O—C—
M_4	23	0.8	H_3C-isopropyl
A_1	23	1.25	b-methylene in a long aliphatic chain
A_2	29.5	1.25	methylene in a long aliphatic chain
E_1	54	3.3	terminal H_3CO-
E_2	56.5	3.75	terminal H_3CO-
E_3	72	3.6	$H_2CO—CH_2$ within an aliphatic chain
ar_1	119	6.6	aromatic CH ortho to oxygen
ar_2	124	7.4	aromatic CH
ar_3	128	7.3	aromatic CH
ar_4	130	7.3	aromatic CH
ar_5	108−111	7.2	aromatic CH
ar_6	131	6.9	aromatic CH

[a] ±0.1 ppm.

HMQC spectra of humic substances can be divided into three areas of chemical shift: aliphatic [$\delta(^{1}H)$, 0.5−3.1 ppm; ^{13}C, 10−50 ppm], heteroatom substituted (^{1}H, 3.1−5.5; ^{13}C, 50−85; including acetals, up to 105 ppm), and aromatic (^{1}H, 6.0−8.0; ^{13}C, 105−145 ppm) CH pairs. Within each area, a manifold of distinct cross-peaks are resolved, some of the most prominent are listed in Table 5. The assignment of the cross-peaks is tentative according to their respective ^{1}H and ^{13}C chemical shift of typical constituents of humic substances.

The HMQC spectra of HA, HAN_2, and HAO_2 are similar in the aliphatic and heteroatom-substituted region. Overall HA and HAN_2 are more closely related than HA and HAO_2 (Figure 5). Within the aliphatic area, resonances with a proton chemical shift <1.1 ppm represent methyl groups; in HA and HAN_2, five distinct methyl resonances each are discernible, while in HAO_2 the cross signals are (in general) less clearly separated. In HAO_2, cross-peaks attributed to alkylated nitrogen (^{1}H, 2.8−3.5; ^{13}C, 40−53) are more prominent than in HA. In the aromatic region of the spectra, ar_1−ar_4 are retained in HA, HAN_2, and HAO_2, while in HAO_2 ar_5 and ar_6 have been vanished.

Complementary information is provided by homonuclear H,H−COSY spectra (Figure 6), where cross signals indicate geminal and vicinal couplings ($^{2,3}J$(HH) > 6 Hz) among protons. According to their range of chemical shift, methyl groups (M, d <1.0), pure aliphatics (A, δ < 1.9), functionalized aliphatics (a, δ 1.9−3.1) and heteroatom-substituted protons (E, δ, 3.1−4.7) are differentiated. In the H,H−COSY spectrum of HAO_2, the methyl groups show five significant cross-peaks, each connecting a methyl resonance to a proton showing $\delta(^{1}H)$ < 1.8 ppm (MA), thus indicating correlations between purely aliphatic hydrogen atoms.

Cross-peaks close to the diagonal relate protons of similar chemical environment, most prominently purely aliphatic protons among themselves (AA) or with protons in a-position to carbonyl or aromatic (or β to hydroxy functions) resonances (Aa). Correlations among oxygen-substituted CH positions (EE) indicate carbohydrate-like structures. Prominent off-diagonal cross-peaks relate methyl groups to aliphatics (MA), oxygen (AE), and substituted aliphatics to ethers (aE).

In the aromatic section of the GS−COSY spectra, a major cross-peak relating aromatic protons with a chemical shift of 6.1 (proton ortho to oxygen substitution) and 7.2 (vicinal proton in meta position and adjacent to C-substitution) has almost disappeared in HAO_2. Sizable changes within the aliphatic framework are indicated by variable cross-peak amplitudes and locations. The higher proportion of protons resonating from 1.9 to 4.7 ppm in HAO_2 as compared to HA (HAO_2, 61%; HA, 51% of total integrated ^{1}H NMR intensity, cf. Table 4) is reflected in substantial enhanced cross-peak amplitudes (aE) within this region of chemical shift. Oxidation within the aliphatic moiety is also indicated by an increase in cross-peak intensity in the chemical shift region ranging from 1.8 to 2.7 (aa).

Pyrolysis-Field Ionization Mass Spectroscopy (Py-FIMS). Py-FIMS spectra of HA and HAN_2 show closely related m/z repartition profiles (Figure 7) with only minor alterations. However in HAN_2 the low molecular weight region exhibits increased relative intensity confirming the decrease in molecular weight due to the disaggregation processes already observed with size exclusion chromatography (Table 2). The quantitative evaluation only showed minor changes. The Py-FIMS profile of the HAO_2 fraction in contrast is very different as compared with the nonirradiated sample and mainly shows low molecular weight fractions similar to the FA fraction as suggested by CZE chromatograms.

FA and HA were volatilized by 60%, higher thermal stability of the latter is indicated by higher temperature representing beginning (220 vs 180 °C) and maximum (380 vs 350 °C) of the TIC. The Py-MS spectra of FA are shifted to smaller mass units as compared to HA in line with a reduced TIC of FA

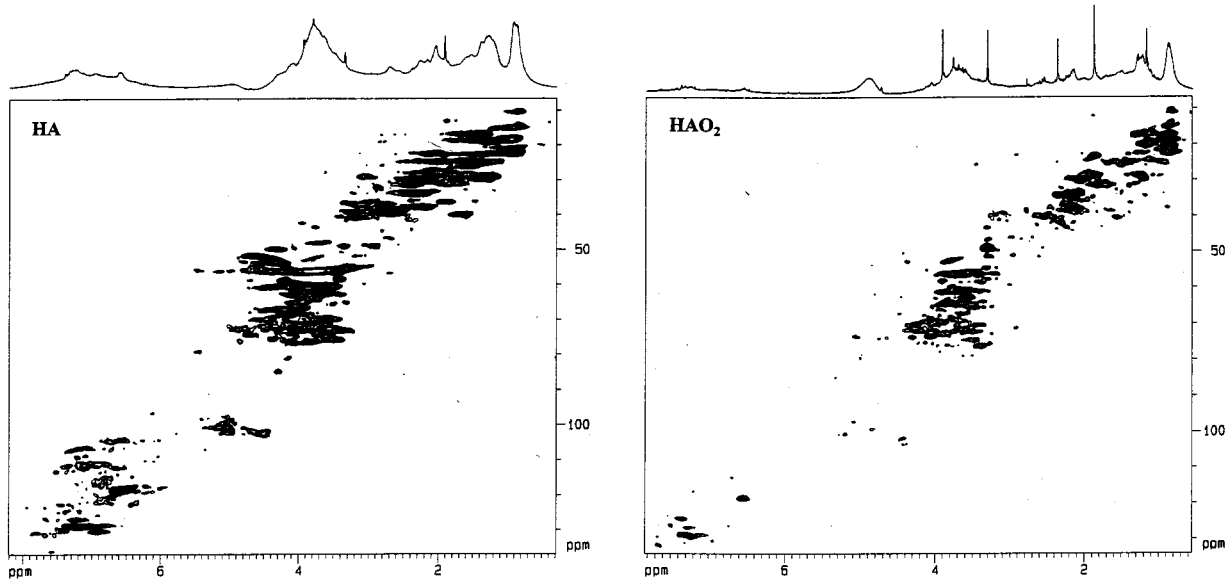

FIGURE 5. GS−HMQC spectra of HA and HAO_2.

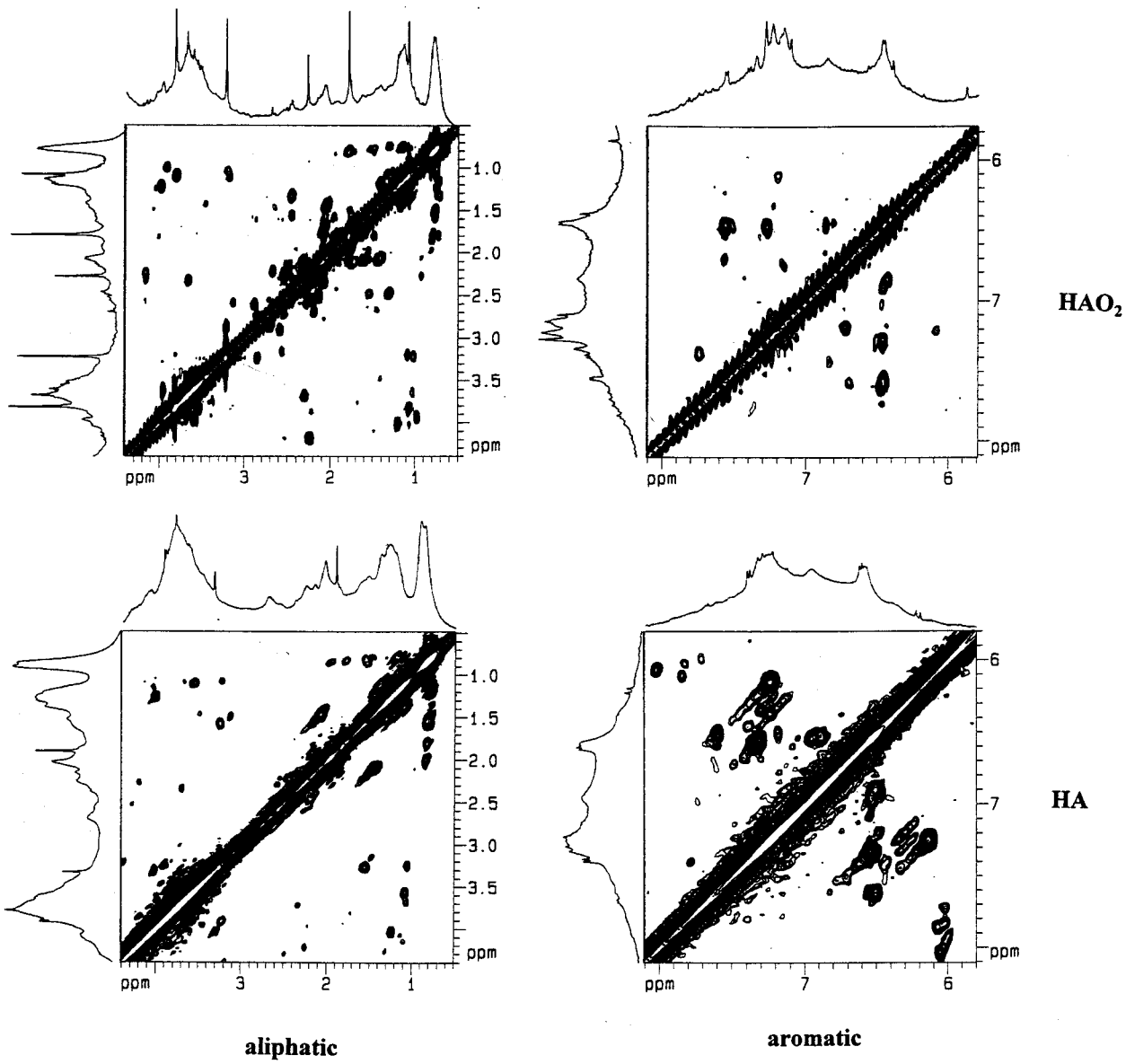

FIGURE 6. GS−H,H−COSY spectra (500 MHz) of HA (lower) and HAO_2 (upper trace); aliphatic (left) and aromatic (right) section.

relative to HA. HAO_2 and HAN_2 were volatilized by 54 and 44%, respectively. The TIC decreased by far more than the carbon content. The comparison of the thermograms indicated no substantial alteration in the thermal stability of HA, HAN_2, and HAO_2. Compared to HA, HAN_2 showed a relative enrichment of carbohydrates [*m*/*z*: 84, 96, 110, 112], lignin monomers [*m*/*z*: 15, 164, 168, 180, 194], and nitrogen compounds; the relative amount of lignin dimers, lipids, and alkyl aromatics decreased. In HAO_2, the oxidative cleavage of higher molecular compounds such as lignin dimers, lipids, and alkyl aromatics decreases the intensity of the higher masses, and an enrichment of carbohydrates [*m*/*z*: 84, 96, 110, 126], lignin monomers [*m*/*z*: 94, 108, 110, 122, 124, 126], and nitrogen compounds [*m*/*z*: 59, 83, 85, 95] is found.

The quantitative evaluation of the structural subunits shows that the carbohydrates, the alkyl aromatics, the N compounds, and peptides are the more stable DHM fractions to photooxidation. The lignin dimers are disappearing, mainly degraded to lignin monomers that are further oxydized. The lipid fraction is also extensively degraded (Figure 8). Comparing the composition of the HAO_2 with FA, the latter exhibits a much higher alkyl aromatic, lignin, and lipid content, even though both compounds display a similar molecular weight distribution and electrophoretic behavior.

Photoreactivity of Humic Structural Fragments. Photobleaching of humic substances during irradiation, which has been described elsewhere (*27*), is pronounced in oxygen atmosphere while virtually absent in nitrogen atmosphere. Both direct, primary, and indirect photoprocesses have been documented in natural waters (*55*). Photon absorption can cause direct photolysis with three primary photoproducts formed: the solvated electron, the cation radical, and triplets (*56*). All remaining photochemistry must depend on the subsequent fate of these primary photoproducts. The potential partner reactive species present at the largest concentrations are humics themselves and dissolved O_2 (2.5×10^{-4} M at saturation). Humic substances sensitize the photoproduction of a variety of transient oxidants such as singlet oxygen (*57, 58*), free and hydroxyl radicals (*59, 60*), hydrated electrons (*61*), hydrogen peroxide (*62, 63*), and peroxy radicals (*64*). In fulvic acids, the primary photoproduct quantum yields in the ultraviolet (*66*) are significantly higher than those deduced from steady-state concentrations of these transient oxidants, which are no more than millimolar. Therefore, reactions with these will take times longer

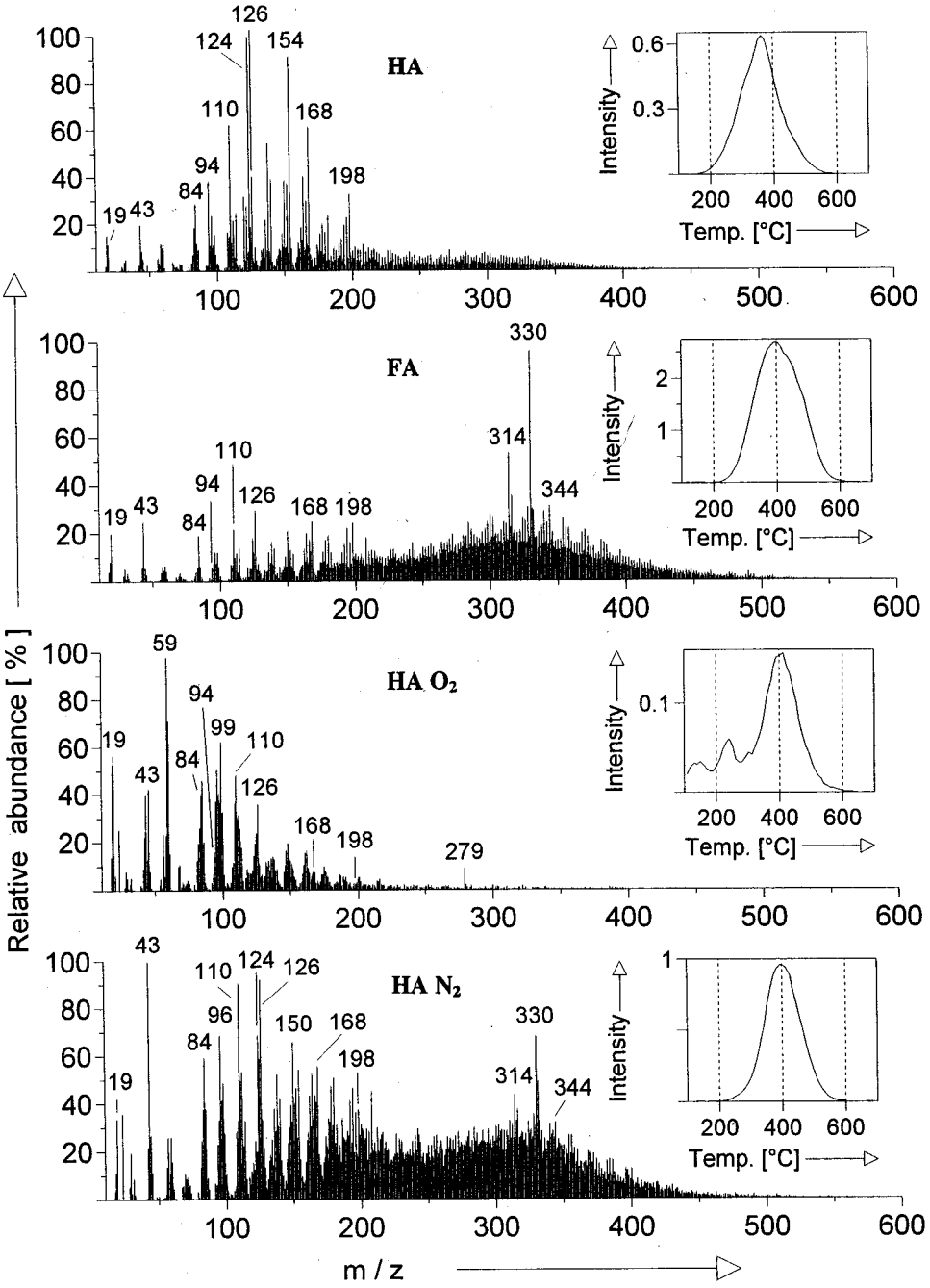

FIGURE 7. Py-FI mass spectra and thermograms (inserted upper right) of FA, HA, HAO_2, and HAN_2.

than microsecondes even for diffusion-limited scavenging; in contrast, reactions within the humic polymer may be quite fast. Chromophore interactions in the humic polymer can slow radiationless decay and offer pathways for intersystem crossing. Most naturally occurring compounds exhibit only weak absorbances, and reactions occurring by direct photolysis are the exceptions rather than the rule (*67*).

It was suggested that aromatic ketones in the exited triplet state could be involved in the transformation of phenolic compounds (*65*), but a recent study showed no direct correlation between photochemical behavior of different synthetic and soil-extracted humic substances and their structural characteristics (*26*).

Common to the photochemistry of humic functional groups comprised from the general formula R(C═O)—X (where X is OH, OR, O(C═O)R, or NHR) is fragmentation with expulsion of carbon monoxide, carbon dioxide, or other small molecules (*68*—*72*). Numerous reaction pathways are available for excited states [homolysis of σ- and π-bonds, heterolysis, ionization, intermolecular oligomerization, intramolecular rearrangement, α- (type a and b) and β-cleavage (type c), but many of the fragmentation reactions observed can be classified with the bond cleavage approach given in Figure 9. Many carboxylic acids undergo photochemical decarboxylation (*73*) and homolytic α-cleavage (type a: the α-bond with the lower homolytic bond strength is expected to break first) seems to be the primary process in the excited state frequently generating O═C—OH radicals. The efficiency of the photodecarboxylation and the resulting product distribution mainly depends on the structure of the reactant (aliphatic, aryl or benzylic carboxyl, or ester group) and the presence or absence of oxygen. In oxygen-free aqueous solutions of acetic acids, the radical O═C—OH is observed (type a), which subsequently loses a hydrogen atom to yield

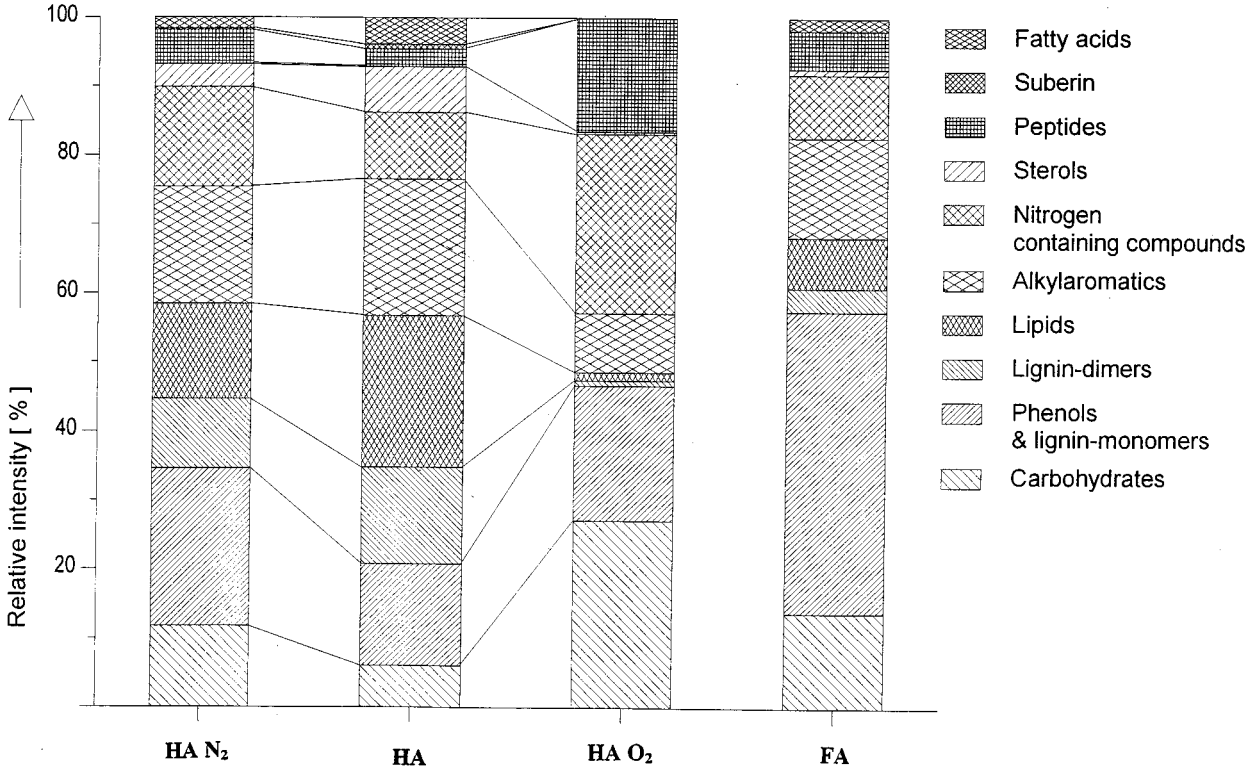

FIGURE 8. Quantitative distribution of structural subunits of FA, HA, HAO_2 and HAN_2 from Py-FI mass spectra.

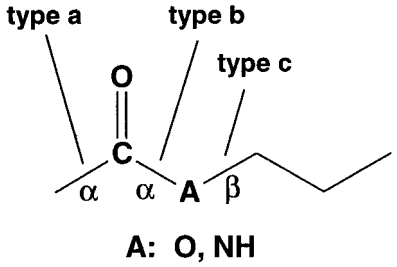

FIGURE 9. General photochemical fragmentation reactions of acids, amides, anhydrides, esters, lactones, and lactams (*70*).

CO_2. Long-chain aliphatic carboxylic acids undergo Norrish type 2 reactions with hydrogen abstraction from the alkyl chain, producing terminal alkenes and acetic acid. Alkenes yield allylic hydroperoxides and/or dioxetanes upon reaction with singlet oxygen and other oxidation products depending on individual substrate (*73*) and may undergo further reactions to give more stable products such as carboxylic acids.

Esters and lactones can undergo α-cleavage of both types a and b upon irradiation; the latter is often followed by decarbonylation. Type c β-cleavage can be facilitated by stabilization of a particular radical; thus benzyl esters normally give benzyl radicals, whereas phenyl esters preferentially undergo α-cleavage (type b) to give resonance stabilized alkoxy radicals. These processes are generally homolytic ones, and the products are those of subsequent radical reactions (*71*). Benzophenone carboxylic acids, for example, were found to oxydize in aqueous solution with nucleophilic OH (radical reactions) followed by β-scission (generation of the aryl radicals) and CO_2 elimination (*75*). Benzoate esters and similar aryl esters undergo Norrish type 2 photoelimination to give the aromatic acid and alkenes (*71, 72*). CO is a major product in the photolysis of formate esters. In aldehydes, ketones, and anhydrides, and less frequently in esters, one of the most common reaction types is the homolysis of the carbonyl-substituent bond (type b), frequently accompanied by decarbonylation. Photodecarbonylation is most frequently observed as a side reaction of the photo-Fries rearrangement, a photochemical conversion of aryl esters into α-aroylphenols with phenols observed as a major byproduct. Phenoxy radicals (long-lived and insensitive to oxygen) and phenoxymethyl radicals (oxygen sensitive, giving CO_2) were reported to arise from photolysis of phenols, methoxylated benzenes, and aryl acids, respectively (*76*). It is known from in vivo radical chemistry that phenoxy radicals are unexpectedly reactive toward phenolic compounds (*77*).

Our results indicate an extensive disappearance of phenolic subunits as well as a substantial synthesis of carboxy acids under oxygen atmosphere. Oxidative degradation of humic substances also occurs via *o*- and *p*-quinone ring-opening reactions (nucleophilic attack of O_2^- on the positively polarized carbon atom of the carbonyl group), followed by formation of two carboxylic groups (*29*). In natural waters the photooxidation of phenols is sensitized by DOM, most probably via electron transfer and H-abstraction reaction rather than by reaction with singlet oxygen (*78, 79*), which was identified as an important photooxidant of phenolate anions in surface waters (*80*). Long living photooxidants of yet unknown structure also contribute to photosensitized oxidation of phenols (*67*). Under oxygen, intermediate radical species may be oxidized to carboxylic acids by the various transient oxidants generated by DOM. Under nitrogen, energy transfer from DOM triplet states within the humic polymer will be more important.

The photodegradation of the soil humic acid under oxygen and nitrogen atmosphere demonstrated that the presence of oxygen is essential for an extensive photooxidation, proving that sensitizing reactions involving reactive oxygen species are predominant. As nearly all of our data show, there is a selective alteration of functional groups during the reaction. The lignin and the lipid constituents are the most affected by photooxidation. The N compounds, the alkyl aromatics, and the carbohydrates were the most stable to these drastic photochemical degradation processes. It is expected that

under milder photochemical conditions, such as in natural environments, the DHM as well as the DOC will behave in an analogous way as observed in the transition from HA to HAO_2 in terms of selective photodegradation and disaggregation phenomena but with slower kinetics.

Photochemical processes should be viewed as decisive factors influencing the chemical structure of natural organic refractory matter. Environmental factors such as season, latitude, time of the day, type of DOC, and depth as well as mixing characteristics of the concerned water body are expected to affect the reactivity and product distribution.

Acknowledgments

The authors want to thank B. Gerard and J. M. Portal from the Centre de Pédologie Biologique (CPB/CNRS, Nancy, France) for the elemental analysis. Financial support by the Deutsche Forschungsgemeinschaft, Bonn-Bad Godesberg (Projects Schu 416/3 and Schu 416/18-3), is gratefully acknowledged.

Literature Cited

(1) Steinberg, C.; Muenster U. In *Humic Substances in Soil, Sediment and Water*; Aiken, G. R., McKnight, D. M., Wershaw, R. L., MacCarthy, P., Eds.; Wiley: New York, 1985.
(2) Thurman, E. M. In *Organic Geochemistry of Natural Waters*; Martinus Nijhoff/Junk Publishers: Dordrecht, 1986.
(3) Malcolm, R. L. *Anal. Chim. Acta* **1990**, *232*, 19−30.
(4) Leenheer, J. A.; Werschaw, R. L.; Reddy, M. M. *Environ. Sci. Technol.* **1995**, *29*, 393−398.
(5) Leenheer, J. A.; Werschaw, R. L.; Reddy, M. M. *Environ. Sci. Technol.* **1995**, *29*, 399−405.
(6) Averett, R. C.; Leenheer, J. A.; McKnight, D. M.; Thorn, K. A. *Humic Substances in the Suwannee River, Georgia: Interactions, Properties, and Proposed Structures*; Open-File Report 87-557; U.S. Geological Survey: Denver, CO, 1987.
(7) Shevchenko, S. M.; Bailey, G. W. *Crit. Rev. Environ. Sci. Technol.* **1996**, *26*, 95−153.
(8) Jardim, W. F.; Campos, M. L. A. M. *Sci. Total Environ.* **1988**, *75*, 243−248.
(9) Pages, J.; Gadel, F. *Sci. Total Environ.* **1990**, *99*, 173−204.
(10) Bothwell, M. L.; Sherbot, D. M. J.; Pollock, C. M. *Science* **1994**, *265*, 97−100.
(11) Mopper, K.; Zhou, X.; Kieber, R. J.; Kieber, D. J.; Sikorski, R. J.; Jones, R. D. *Nature* **1991**, *353* (5), 60−63.
(12) Salonen, K.; Vähätalo, A. *Environ. Int.* **1994**, *20*, 307−312.
(13) Valentine, R. L.; Zepp, R. G. *Environ. Sci. Technol.* **1993**, *27*, 409−413.
(14) Schindler, D. W.; Curtis, P. J.; Parker, B. R.; Stainton, M. P. *Nature* **1996**, *379*, 705−708.
(15) Wetzel, R. G.; Hatcher, P. G.; Bianchi, T. S. *Limnol. Oceanogr.* **1995**, *40*, 1369−1380.
(16) Kieber, J. K.; Zhou, X.; Mopper, K. *Limnol. Oceanogr.* **1990**, *35*, 1503−1515.
(17) Choudhry, G. G. In *Humic substances—Photophysical and free radical aspects and interactions with environmental chemicals*; Gordon and Breach Science Publishers: New York, 1984.
(18) Frimmel, F. H. *Environ. Int.* **1994**, *20*, 373−385.
(19) Khan, S. U.; Schnitzer, M. *J. Environ. Sci. Health* **1978**, *B13*, 299−310.
(20) Hermann, R.; Ziechmann, W. *Z. Pflanzenernähr. Bodenk.* **1988**, *151*, 219−220.
(21) Minero, C.; Pramauro, E.; Pelizzeti, E.; Dolci, M.; Marchesini, A. *Chemosphere* **1992**, *24*, 1597−1606.
(22) Klöpffer, W. *Sci. Total Environ.* **1992**, *123/124*, 145−159.
(23) Schmitt, Ph.; Freitag, D.; Sanlaville, Y.; Lintelmann, J.; Kettrup, A. *J. Chromatogr. A* **1995**, *709*, 215−225.
(24) Nick, K.; Schöler, H. F.; Mark, G.; Söylemez, T.; Akhlaq, M. S.; Schumann, H. P.; Von Sontag *J. Water SRT−Aqua* **1992**, *41*, 82−87.
(25) Ollis, D. F.; Pelizzetti, E.; Serpone, N. *Environ. Sci. Technol.* **1991**, *25*, 1523−1529.
(26) Aguer, J. P.; Richard, C.; Andreux, F. *J. Photochem. Photobiol. A: Chem.* **1996**, *103*, 163−168.
(27) Gjessing, E. T. In *Physical and Chemical Characteristics of Aquatic Humus*; Ann Arbor Science Publishers Inc.: Ann Arbor, MI, 1976; pp 85−89.
(28) Orlow, D. S.; et al. *Acad. Sci. Kirgisia CCP* **1976**, *2*, 53−58.
(29) Choudhry, G. G. *Toxicol. Environ. Chem.* **1981**, *4*, 261−295.
(30) Frimmel, F. H.; Bauer, H. *Sci. Total Environ.* **1987**, *62*, 139−148.
(31) Kotzias, D.; Herrmann, M.; Zsolnay, A.; Beyerle-Pfnür, R.; Parlar, H.; Korte, F. *Chemosphere* **1987**, *16*, 1463−1468.
(32) Slawinski, J.; Pzyna, W.; Slawinska, D. *Photochem. Photobiol.* **1978**, *28*, 459−463.
(33) Gerasimowicz, W. V.; Byler, D. M.; Susi, H. *Appl. Spectrosc.* **1986**, *40*, 504−507.
(34) Manny, B. A.; Miller, M. C.; Wetzel, R. G. *Limnol. Oceanogr.* **1971**, *16*, 71−85.
(35) Campanella, L.; Cardarelli, E.; Ferri, T.; Petronio, B. M.; Pupella, A. *Sci. Total Environ.* **1988**, *76*, 41−48.
(36) Baklund, P. *Chemosphere* **1992**, *25* (129), 1869−1878.
(37) Allard, B.; Boren, H.; Petterson C.; Zhang. *Environ. Int.* **1994**, *20*, 97−101.
(38) Dahlen, J.; Bertilsson, S.; Petterson, C. *Environ. Int.* **1996**, *22*, 501−506.
(39) Schmitt, Ph.; Garrison, A. W.; Freitag, D.; Kettrup, A. *Water Res.* **1997**, *31*, 2037−2049.
(40) Schmitt, Ph.; Garrison, A. W.; Freitag, D.; Kettrup, A. *Fresenius' J. Anal. Chem.* **1996**, *354*, 915−920.
(41) Schmitt, Ph.; Trapp, I.; Garrison, A. W.; Freitag, D.; Kettrup, A. *Chemosphere* **1997**, *35*, 55−75.
(42) Scharf, H. D.; Fleischhauer, J.; Aretz, J. In *Methoden der organischen Chemie*; Müller, E., Ed.; Vol. IV5a, Photochemie, Teilband 1; Georg Thieme Verlag: Stuttgart, 1975; pp 41−86.
(43) Garrison, A. W.; Schmitt, Ph.; Kettrup, A. *Water Res.* **1995**, *29*, 2149−2159.
(44) Belton, P. S.; Cox, I. J.; Harris, R. K. *J. Chem. Soc., Faraday Trans.* **1985**, *81*, 63−75.
(45) Croasmun, W. R., Carlson, R. M. K., Eds. In *Two-Dimensional NMR Spectroscopy*; VCH Publishers Inc.: Weinheim, 1994.
(46) Shin, H. S.; Moon, H. *Soil Sci.* **1996**, *161*, 250−256.
(47) Schulten, H.-R. *J. Anal. Appl. Pyrol.* **1987**, *12*, 149−186; **1993**, *25*, 97−122.
(48) Coxon, J. M.; Halton, B. In *Organic Photochemistry*; Cambridge University Press: Cambridge, 1974.
(49) Chen, Y.; Senesi, N.; Schnitzer, M. *Soil Sci. Soc. Am. J.* **1977**, *41*, 352−357.
(50) Amalay, M.; Bussieres, D. In *Humic Substances and Organic Matter in Soil and Water Environments*; Clapp, C. E., Hayes, M. H. B., Senesi, N., Griffith, S. M., Ed.; International Humic Substances Society, University of Minnesota: Madison, 1996; pp 251−265.
(51) Malcolm, R. L. *Anal. Chim. Acta* **1990**, *232*, 19−30.
(52) Kessler, H.; Gehrke, M.; Griesinger, C. *Angew. Chem.* **1988**, *100*, 507−544; *Angew. Chem., Int. Ed. Engl.* **1988**, *27*, 490−536.
(53) Lambert, J.; Burba, P.; Buddrus, J. *Magn. Reson. Chem.* **1992**, *30*, 221−227.
(54) Kretchmer, A.; Lambert, J.; Buddrus, J.; Jancke, H. *Erdoel, Erdgas, Kohle* **1995**, *111*, 524−525.
(55) Cooper, W. J.; Zika, R. G.; Pestane, R. G.; Fischer, A. M. In *Aquatic humic substances; Influence on fate and treatment of pollutants*; Suffet, I. H., MacCarthy, P., Ed.; Advances in Chemistry Series 219; American Chemical Society: Washington, DC, 1987; pp 333−362.
(56) Zepp, R. G.; Schlotzhauer, P. F.; Sink, R. M. *Environ. Sci. Technol.* **1985**, *19*, 74−81.
(57) Zepp, R. G.; Lee Wolfe, N.; Baughman, G. L.; Hollis, R. C. *Nature* **1977**, *267*, 421−423.
(58) Haag, W. R.; Hoigné, J. *Environ. Sci. Technol.* **1986**, *20*, 341−348.
(59) Mill, T.; Hendry, D. G.; Richardson, H. *Science* **1980**, *207*, 886−887.
(60) Zafiriou, O. C. *Nature* **1987**, *325*, 481−482.
(61) Zepp, R. G.; Braun, A. M.; Hoigné, J.; Leenheer, J. A. *Environ. Sci. Technol.* **1987**, *21*, 485.
(62) Cooper, W. J.; Zika, R. G. *Science* **1983**, *220*, 711−712.
(63) Cooper, W. J.; Zika, R. G.; Pestane, R. G.; Plane, J. M. C. *Environ. Sci. Technol.* **1988**, *22*, 1156−1160.
(64) Zepp, R. G.; Baughman, G. L.; Schlotzhauer, P. F. *Chemosphere* **1981**, *10*, 119−126.
(65) Draper, W. M.; Crosby, D. G. *J. Agric. Food Chem.* **1981**, *29*, 699−702.
(66) Draper, W. M.; Crosby, D. G. *Arch. Environ. Contam. Toxicol.* **1983**, *12*, 121−126.
(67) Canonica, S.; Hoigné, J. *Chemosphere* **1995**, *30*, 2365−2374.
(68) Bruccoleri, A.; Pant, B. C.; Sharma, D. K.; Langford, C. H. *Environ. Sci. Technol.* **1993**, *27*, 889−894.
(69) Zika, R. G.; Cooper, W. J. In *Photochemistry of Environmental Aquatic Systems*; ACS Symposium Series 327; American Chemical Society: Washington, DC, 1985.

(70) Givens, R. S.; Levi, N. In *The Chemistry of Acid Derivatives, Supplement B*, Vol. 2; Patai, S., Ed.; Wiley: New York, 1992; pp 641−752.
(71) Coyle, J. D. *Chem. Rev.* **1978**, *78*, 97−123.
(72) Suginome, H. In *The Chemistry of Acid Derivatives, Supplement B*, Vol. 2; Patai, S., Ed.; Wiley: New York, 1992; pp 1107−1160.
(73) Bockman, T. M.; Hubig, S. M.; Kochi, J. K. *J. Am. Chem. Soc.* **1996**, *118*, 4502−4503.
(74) Gorman, A. A. *Adv. Photochem.* **1992**, *17*, 217−274.
(75) Säuberlich, J.; Brede, O.; Beckert, D. *J. Phys. Chem.* **1996**, *100*, 18101−18107.
(76) Power, J. F.; Sharma, D. K.; Langford, C. H.; Bonneau R.; Joussot-Dubien, J. *Photochem. Photobiol.* **1986**, *44* (1), 11−13.
(77) Foti, M.; Ingold, K. U.; Lusztyk, J. *J. Am Chem. Soc.* **1994**, *116*, 9440−9447.
(78) Canonica, S.; Jans, U.; Stemmler, K.; Hoigné, J. *Environ. Sci. Technol.* **1995**, *29*, 1822−1831.
(79) Faust, B. C.; Hoigné J. *Environ. Sci. Technol.* **1987**, *21*, 957−964.
(80) Tratnyek, P. G.; Hoigné J. *Environ. Sci. Technol.* **1991**, *25*, 1596−1604.

Received for review July 21, 1997. Revised manuscript received March 27, 1998. Accepted May 11, 1998.

ES970636Z